Astronomy & Astrophysics manuscript no. Lardo˙v5˙lang˙saga
November 19, 2014
© ESO 2014

arXiv:1411.4886v1 [astro-ph.GA] 18 Nov 2014

The Gaia-ESO Survey: Kinematics of seven Galactic globular clusters⋆

C. Lardo[1,2], E. Pancino[2,3] , M. Bellazzini[2] , A. Bragaglia[2] , P. Donati[2], G. Gilmore[4], S. Randich[5], S. Feltzing[6], R. D. Jeffries[7] , A. Vallenari[8], E. J. Alfaro[9] , C. Allende Prieto[10,11], E. Flaccomio[12], S. E. Koposov[4,13], A. Recio-Blanco[14], M. Bergemann[4], G. Carraro[15], M. T. Costado[9], F. Damiani[12], A. Hourihane[4], P. Jofré[4], P. de Laverny[14] , G. Marconi[15], T. Masseron[4], L. Morbidelli[5], G. G. Sacco[5] ,C. C. Worley[4]

[1] Astrophysics Research Institute, Liverpool John Moores University, 146 Brownlow Hill, Liverpool L3 5RF, United Kingdom e-mail: C.Lardo@ljmu.ac.uk
[2] INAF - Osservatorio Astronomico di Bologna, via Ranzani 1, 40127, Bologna, Italy
[3] ASI Science Data Center, Via del Politecnico SNC, 00133 Roma, Italy
[4] Institute of Astronomy, University of Cambridge, Madingley Road, Cambridge CB3 0HA, United Kingdom
[5] INAF - Osservatorio Astrofisico di Arcetri, Largo E. Fermi 5, 50125, Florence, Italy
[6] Lund Observatory, Department of Astronomy and Theoretical Physics, Box 43, SE-221 00 Lund, Sweden
[7] Astrophysics Group, Research Institute for the Environment, Physical Sciences and Applied Mathematics, Keele University, Keele, Staffordshire ST5 5BG, United Kingdom
[8] INAF - Padova Observatory, Vicolo dell'Osservatorio 5, 35122 Padova, Italy
[9] Instituto de Astrofísica de Andalucía-CSIC, Apdo. 3004, 18080, Granada, Spain
[10] Instituto de Astrofísica de Canarias, E-38205 La Laguna, Tenerife, Spain
[11] Universidad de La Laguna, Dept. Astrofísica, E-38206 La Laguna, Tenerife, Spain
[12] INAF - Osservatorio Astronomico di Palermo, Piazza del Parlamento 1, 90134, Palermo, Italy
[13] Moscow MV Lomonosov State University, Sternberg Astronomical Institute, Moscow 119992, Russia
[14] Laboratoire Lagrange (UMR7293), Université de Nice Sophia Antipolis, CNRS,Observatoire de la Côte d'Azur, CS 34229,F-06304 Nice cedex 4, France
[15] European Southern Observatory, Alonso de Cordova 3107 Vitacura, Santiago de Chile, Chile

Received XXX XX, XXXX; accepted XXX XX, XXXX

ABSTRACT

The Gaia-ESO survey is a large public spectroscopic survey aimed at investigating the origin and formation history of our Galaxy by collecting spectroscopy of representative samples (about 10^5 Milky Way stars) of all Galactic stellar populations, in the field and in clusters. The survey uses globular clusters as intra- and inter-survey calibrators, deriving stellar atmospheric parameters and abundances of a significant number of stars in clusters, along with radial velocity determinations. We used precise radial velocities of a large number of stars in seven globular clusters (NGC 1851, NGC 2808, NGC 4372, NGC 4833, NGC 5927, NGC 6752, and NGC 7078) to validate pipeline results and to preliminarily investigate the cluster internal kinematics. Radial velocity measurements were extracted from FLAMES/GIRAFFE spectra processed by the survey pipeline as part of the second internal data release of data products to ESO. We complemented our sample with ESO archival data obtained with different instrument configurations. Reliable radial velocity measurements for 1513 bona fide cluster star members were obtained in total. We measured systemic rotation, estimated central velocity dispersions, and present velocity dispersion profiles of all the selected clusters, providing the first velocity dispersion curve and the first estimate of the central velocity dispersion for the cluster NGC 5927. Finally, we explore the possible link between cluster kinematics and other physical parameters. The analysis we present here demonstrates that Gaia-ESO survey data are sufficiently accurate to be used in studies of kinematics of stellar systems and stellar populations in the Milky Way.

Key words. globular clusters: general

1. Introduction

Globular clusters (GCs) have always been regarded as unique laboratories to explore many aspects of stellar dynamics (Meylan & Heggie 1997). In a first approximation, they can be considered spherically symmetric, non-rotating, and isotropic; but, as improved observations and new theoretical studies have become available, it became clear that they are complex (see Zocchi et al. 2012, Bianchini et al. 2013, and Kacharov et al. 2014 for a discussion). In particular, radial anisotropy (Ibata et al. 2013), deviations from sphericity (White & Shawl 1987; Chen & Chen 2010), mass segregation (Da Costa 1982), signatures of core-collapse (Djorgovski & King 1984), and velocity

⋆ Based on data products from observations made with ESO telescopes at the La Silla Paranal Observatory under programme 188.B-3002 (the public Gaia-ESO spectroscopic survey, PIs Gilmore & Randich) and on the archive data of the programmes 62.N-0236, 63.L-0439, 65.L-0561, 68.D-0212, 68.D-0265, 69.D-0582, 064.L-0255, 065.L-0463, 071.D-0205, 073.D-0211, 073.D-0695, 075.D-0492, 077.D-0246, 077.D-0652, 079.D-0645, 080.B-0489, 080.D-0106, 081.D-0253, 082.B-0386, 083.B-0083, 083.D-0208, 083.D-0798, 085.D-0205, 086.D-0141, 088.A-9012, 088.B-0403, 088.B-0492, 088.D-0026, 088.D-0519, 089.D-0038, 164.O-0561, 386.D-0086.

dispersion inflated by unresolved binary stars (Bradford et al. 2011) have been observed and need to be explained in the framework of a dynamical scenario.

Different physical mechanisms may determine these deviations from the perfect sphere: velocity anisotropies, tidal stresses, and internal rotation (Goodwin 1997; Gnedin et al. 1999; van den Bergh 2008; Bianchini et al. 2013; Kacharov et al. 2014). The idea that internal rotation plays a fundamental part in determining the morphology of GCs was formulated some 50 years ago (King 1961). Internal rotation has been detected in a growing number of GCs from line-of-sight velocity measurements (see, e.g., Bellazzini et al. 2012, hereafter B12) and, in a few cases, from proper motion measurements (e.g., van Leeuwen et al. 2000; Anderson & King 2003). The interest in the GC internal rotation is manifold. Analytical (Longaretti & Lagoute 1997), Fokker-Planck (Spurzem & Einsel 1999), and N-body models (Ernst et al. 2007) demonstrated that an overall (differential) rotation has a noticeable influence on stellar systems that evolve by two-body relaxation. In particular, it accelerates the core-collapse time scales (Ernst et al. 2007)[1]. Internal rotation may also play an indirect role in the open question of whether there are intermediate-mass black holes (IMBH) in some GCs. In fact, the detection of strong gradients in the velocity dispersion profile toward the cluster core is often interpreted as a hint of the presence of an IMBH (Baumgardt et al. 2005), but the evidence gathered so far in support of the existence of IMBHs is inconclusive and controversial, and none of the published studies (van der Marel & Anderson 2010; Lützgendorf et al. 2011; Lanzoni et al. 2013) did consider differential rotation, which, together with anisotropy, can yield gradients in the velocity dispersion profiles (Varri & Bertin 2012; Bianchini et al. 2013). Finally, recent investigations indicate that rotation could be a key ingredient in the formation of multiple generations of stars in GCs (Bekki 2010; Mastrobuono-Battisti & Perets 2013).

In this science verification paper, we make use of the Gaia-ESO survey radial velocity determination to perform a kinematic analysis for seven Galactic GCs (NGC 1851, NGC 2808, NGC 4372, NGC 4833, NGC 5927, NGC 6752, and M15), following the same scheme as B12. The samples we analyse were collected for a completely different scientific purpose, therefore they present intrinsic limitations for the characterisation of the cluster kinematics. The most recent dedicated studies used up to several hundred radial velocity determinations (see e.g., Lane et al. 2009, 2010a,b), in some cases complemented with proper motions (van de Ven et al. 2006; van den Bosch et al. 2006; McLaughlin et al. 2006; Watkins et al. 2013), while we have V_r determinations for fewer than 100 stars for some clusters (i.e., NGC 2808, NGC 4833, NGC 5927). Furthermore, the cluster members are unevenly distributed with radius within each cluster, with the large majority of the stars lying at distances greater than the half-light radius, because it is difficult to allocate fibers in the very crowded central regions.

Still, our analysis *(a)* provides a validation of the Gaia-ESO survey radial velocities in a controlled sample, *(b)* provides (and makes publicly available) additional observational material to study the kinematics of the considered clusters, and *(c)* at least in one case, NGC 5927, provides the first insight into the cluster kinematics.

This paper is structured as follows: We begin by describing the data and the membership selection for each cluster in Sect. 2. We compute systemic velocities and velocity dispersions in Sect. 3, as well as rotations (in Sect. 4). In Sect. 5 we investigate the links between kinematics and cluster parameters. Finally, our concluding remarks are presented in Sect. 6.

2. Sample and radial velocity measurements

2.1. Data sets

The Gaia-ESO Survey is a public spectroscopic survey that uses the FLAMES multi-object spectrograph on the VLT UT-2 (Kueyen) telescope to obtain high-quality, uniformly calibrated spectroscopy of 100 000 stars in the Milky Way (Gilmore et al. 2012, Randich et al. 2013). The survey targets stars in the halo, bulge, thick and thin discs, and in star-forming regions and open clusters to characterize the chemistry and kinematics of these populations. When combined with precise astrometry from the recently launched Gaia satellite (Perryman et al. 2001), the enormous dataset will provide three-dimensional spatial distribution and kinematics, stellar parameters, and chemical abundances for a significant number of stars in the Galaxy.

In addition to the main targets, the Gaia-ESO survey is observing GCs as intra- and inter-survey astrophysical calibrators, deriving stellar atmospheric parameters, abundances, and radial velocities (V_r) for typically a hundred red giant branch (RGB) stars in each cluster. GCs were selected among those used by other surveys as RAVE (Steinmetz et al. 2006; Zwitter et al. 2008; Siebert et al. 2011; Lane et al. 2011), GALAH (Zucker et al. 2013), and APOGEE (Frinchaboy et al. 2012, 2013a,b; Mészáros et al. 2013) where possible. The photometric catalogues for the selected clusters are generally based on UBVI archival images, collected at the Wide-Field Imager (WFI) at the 2.2-m ESO-MPI telescope. The WFI covers a total field of view of $34' \times 33'$, consisting of 8, 2048×4096 EEV-CCDs with a pixel size of $0.238''$. These images were pre-reduced using the IRAF package MSCRED (Valdes 1998), while the stellar photometry was derived by using the DAOPHOT II and ALLSTAR programs (Stetson 1987, 1992). Details on the preproduction, calibration, and full photometric catalogues will be published elsewhere. We thus created the initial sample that includes as many clusters as possible from the other surveys, and filled in the gaps in [Fe/H] with clusters visible from the South that have public photometry data. To select the targets within each cluster, we generally observed RGB stars and performed a survey of FLAMES data in the ESO archive and in the literature (when available) to select probable members. To maximise our chances of obtaining reliable parameters for GC, we gave highest priority to GIRAFFE targets that already had archival observations in different setups and avoided repeating stars that already had UVES observations in the Gaia-ESO survey setups. Additional details of the cluster selection criteria and observational strategy will be given in a forthcoming paper (Pancino et al., in preparation).

Our sample consists of seven Galactic GCs observed by the Gaia-ESO survey. The observations were performed between December 2011 and September 2013 and consist of one pointing for each GC, using the two FLAMES-GIRAFFE[2] setups that are used to observe the main field targets of the survey (Gilmore et al. 2012; Randich et al. 2013): the high-resolution setups HR 10 (centred on 5488Å, with a spectral resolution R=19800) and HR 21 (centred on 8757Å, with a spectral resolution R=16200).

[1] This effect seems to vanish for isolated two-mass N-body models (Ernst et al. 2007).

[2] We considered only stars observed with GIRAFFE to preserve homogeneity.

Table 1. Archive spectra inventory. Note that the number of spectra quoted here is the total number of spectra obtained before Galactic contaminants were removed.

Target	Type	HR4 427.2	HR9A 525.8	HR9B 525.8	HR10 548.8	HR11 572.8	HR13 627.3	HR14A 651.5	HR14B 651.5	HR15N 665.0	HR19A 805.3	HR21 875.7
M 15	Archive					83	155	81				
	Gaia-ESO				79							80
NGC 1851	Archive		104	204		105	196				83	
	Gaia-ESO				94							92
NGC 2808	Archive						113	113			120	
	Gaia-ESO				65							63
NGC 4372	Archive						234	122				
	Gaia-ESO				103							103
NGC 4833	Archive					112	114					
	Gaia-ESO				81							81
NGC 5927	Gaia-ESO				110							110
NGC 6752	Archive	121		99	100	429	515		99	233		231
	Gaia-ESO				108							108

As the Gaia-ESO survey is a public ESO spectroscopic survey, raw spectra are available in the ESO archive[3] as soon as targets are observed. Pipeline-reduced spectra for a fraction of the target stars observed in the first six months of observations are already available at the address `http://archive.eso.org/wdb/wdb/adp/phase3_main/form`. Part of the data analysed in this paper are included in the second internal release and will become public within a few months. In addition to the Gaia-ESO survey spectra, we complement our dataset with archive FLAMES data observed with different instrumental configurations[4].

The GES and archival spectra were processed by the survey pipeline (see Lewis et al., in preparation) and stored at the Cambridge Astronomical Survey Unit (CASU) Gaia-ESO Survey Archive (see Table 1 for a summary). We present in Figs. 1 and 2 the spatial distribution and the location on the cluster colour-magnitude diagrams of the sampled stars.

While expanding our initial dataset, this exercise also allows us to validate the results delivered by the survey data reduction pipeline. We have for the entire sample at least two independent V_r estimates from observations with different instrument settings that we can use to check the internal consistency and accuracy of the derived radial velocities. While complementing our data with archive data, we limited ourselves to samples that were already incorporated by the Gaia-ESO survey pipeline when we started this analysis (February 2014). To maintain the highest accuracy in the radial velocity estimates and the best homogeneity in the velocity zero points, we included only samples of RGB stars that had stars in common with the available sample of stars observed with the HR10 grating that is the basis of our velocity scale (see below).

The data stored at the CASU Gaia-ESO Survey Archive are in multi-extension FITS files that contain both images with spectral data and tables with meta-data and derived information about each object, including radial heliocentric line-of-sight velocity measurements we used throughout this paper. In particular, radial velocities are measured using a two-steps approach.

The V_r determination is based on a procedure described in Koposov et al. (2011). It uses direct per-pixel χ^2 fitting of the spectra by templates. The main ingredient of the procedure is the generation of the model spectrum, given log g, T_{eff}, [Fe/H],

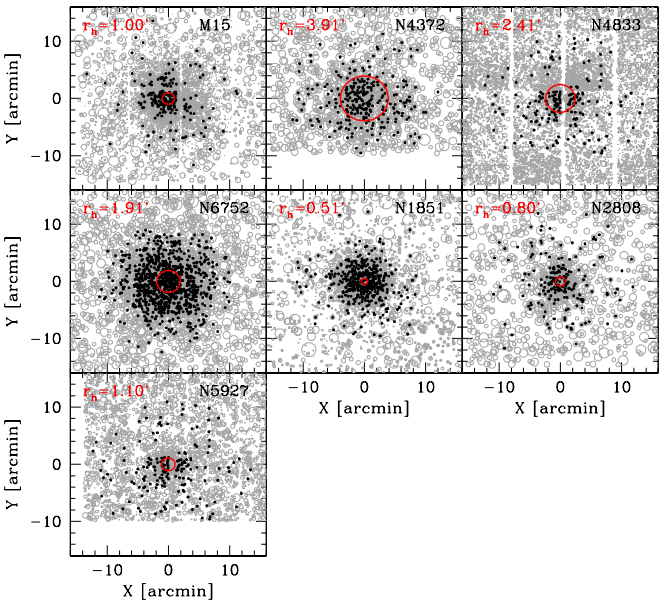

Fig. 1. Spatial distribution of the initial sample (black dots) overlaid on our WFI photometry (grey circles). The half-light radius (from Harris 1996; 2010 edition) is also reported and plotted as a red line. Note that the stars plotted here are all the stars retrieved from the CASU archive before Galactic contaminants were removed and sample selection was made (see text).

and rotational velocity of the star V_{rot}. For this purpose we used the template grid computed at high resolution by Munari et al. (2005). The initial step of the V_r determination is the cross-correlation with the subset of templates. This step is only required to obtain a better initial guess of the V_r and template for subsequent fit. The next step consists of a process of iteratively improving the stellar template and V_r by direct modelling. The process of improving the template involves keeping the radial velocity fixed while performing the downhill Simplex (Nelder & Mead 1965) optimisation of χ^2 by improving stellar parameter estimates: log g , T_{eff}, [Fe/H], and V_{rot}. After this process has converged, we perform the V_r optimisation by evaluating the template on a grid of radial velocities and computing the χ^2 as a function of radial velocity. Then the stellar parameter step and RV steps are repeated a few times until convergence. The calculation of the χ^2 for each log g, T_{eff}, [Fe/H], V_{rot} and V_r

[3] `http://archive.eso.org/eso/eso_archive_main.html`

[4] See `http://www.eso.org/sci/facilities/paranal/instruments/flames/inst/specs1.html` for an updated list and description of the GIRAFFE gratings currently used.

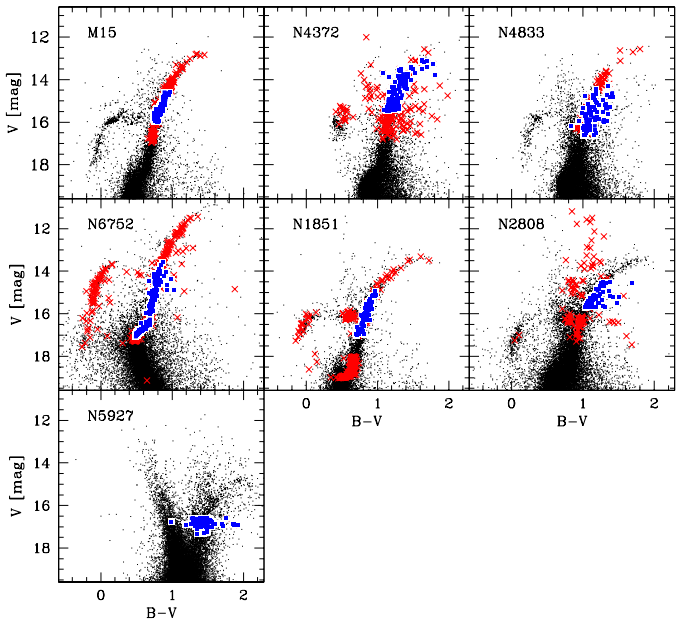

Fig. 2. Gaia-ESO survey targets (blue squares) and GIRAFFE/FLAMES archival data (red crosses) overplotted on our WFI photometry (black dots).

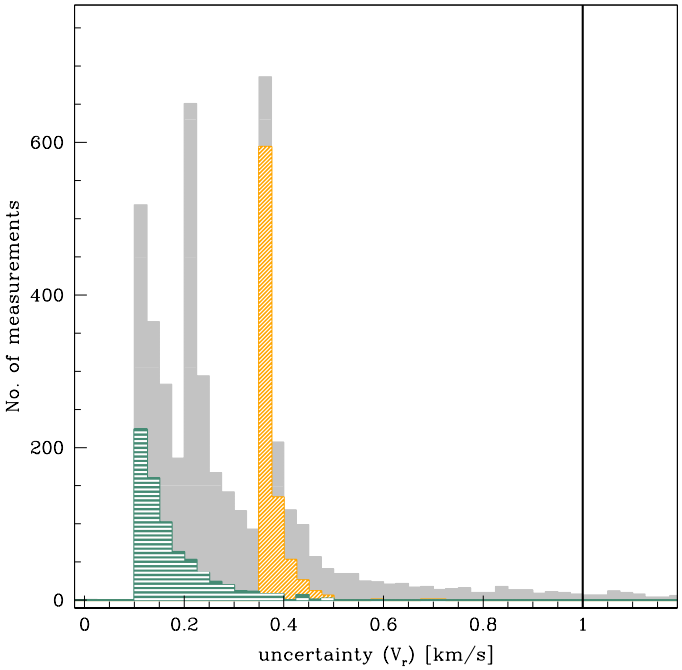

Fig. 3. Distribution of velocity pipeline internal uncertainties associated with each V_r measurement, grey histogram, for all the considered settings, of HR 10, green histogram shaded at 0 degrees, and for HR 21, yellow histogram, shaded at 45 degrees. The vertical line is the adopted threshold for rejecting objects (see text).

also involves simultaneous continuum determination (Koposov et al. 2011), where the observed spectrum is assumed to be the multiplication of the template and a fixed-degree polynomial of the wavelength. As a result of the procedure, we derive χ^2 as a function of V_r for the best-fit template, from which the pipeline determines the V_r estimate and its uncertainty (see also Jeffries et al. 2014).

2.2. V_r estimates from repeated measurements

As there are several stars in common between the observational datasets with different setups, we can check the internal consistency of the radial velocities delivered by the survey pipeline. The mean (median) uncertainty value on individual pipeline V_r estimates is of 0.17 (0.15) and 0.38 (0.37) km s^{-1} (*rms* = 0.07 and 0.05, stars=731 and 830) for the two Gaia-ESO setups HR 10 and HR 21, respectively (see Figure 3). The vast majority of the spectra (≃92%) have uncertainties on $V_r \leq 1.0$ km s^{-1}, ≃84% ≤ 0.5 km s^{-1}, small enough to not affect the measurement of the internal kinematics of the clusters. We decided to adopt a conservative threshold (uncertainty on $V_r \leq 1$ km s^{-1}) to select the stars in the following analysis.

The comparison between the V_r estimates obtained from HR 10 and the other GIRAFFE setups for stars with uncertainty on $V_r \leq 1.0$ km s^{-1} is shown in Fig. 4 for all clusters. Velocities from HR 10 were chosen as a reference because this setup is used, together with HR 21, to observe all the stars targeted by Gaia-ESO survey, and their associated uncertainties are typically smaller than those of HR 21. The mean difference and the standard deviation of the difference between the two sets of estimates with different setups are reported in Table 2. The table also lists the number of stars in common between HR 10 and a given setup. Although the consistency among the different sets of measures is good (i.e., $\Delta V_r \leq 1.0$ km s^{-1}), we note that there are differences in the V_r zero point (see also Donati et al. 2014). This might be due to the fact that Gaia-ESO survey HR 10 observations are generally interleaved with a short exposure in which five dedicated fibres were illuminated by a bright (compared to the stellar spectra) thorium-argon (ThAr) lamp (see also Jeffries et al. 2014). These short exposures (*simcal* observations), combined with much longer day-time ThAr lamp exposures that illuminated all the instrument fibres, are used to adjust both the localisation and the wavelength solution, resulting in a higher precision in radial velocity determinations. However, the differences in the zero-point between the ten V_r sets are not a reason for concern in the present analysis. In some cases, the comparison is based on only a handful of stars (see Fig. 2), but because we did not detect trends and/or large spreads in the ΔV_r, we decided to include these setups in the following analysis as well. The typical precision, as measured from the *rms* of each set of ΔV_r computed after recursive clipping of the very few 3σ outliers is ≤ 1.6 km s^{-1}, but typically much lower than this, about 0.3 km s^{-1}, which is more than satisfying for our purpose here. The actual uncertainty on the single measure should be smaller than the *rms* of ΔV_r because the latter includes the uncertainties of both estimates, added in quadrature.

As a final step, we transformed all radial velocities into the HR 10 system by applying the shifts listed in Table 2 and weighting them by their uncertainty to derive the final V_r. In the case of a single V_r determination we assigned the corrected V_r value to the star along with the formal uncertainty associated with the single measure.

As an additional validation of our final V_r, we compared our determinations with those in the existing literature for NGC 6752, NGC 1851, and NGC 5927. For NGC 6752, we found 159 stars in common with the sample presented by Lane et al. (2010b), and for these stars we measured a mean difference V_r (this paper) - V_r(Lane) of –0.95, σ=1.90 km s^{-1}. For NGC 1851 we have 104 stars in common with Carretta et al. (2010). Our V_r determinations agree well with those from these authors (ΔV_r =

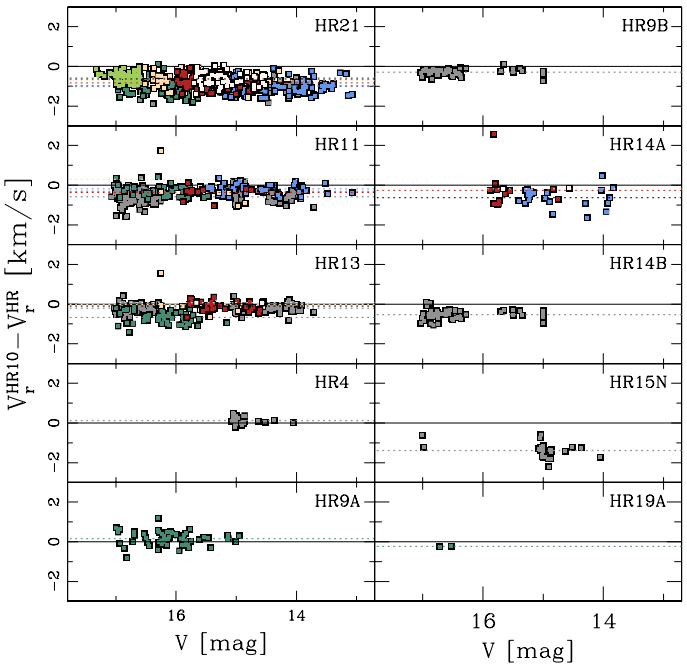

Fig. 4. Comparison between the V_r estimated from spectra obtained with HR10 and other GIRAFFE setups. Different colours correspond to different clusters: M15 (red), NGC 4372 (light blue), NGC 4833 (apricot), NGC 6752 (grey), NGC 1851 (green), NGC 2808 (ivory), and NGC 5927 (light green). The dotted lines indicate the mean difference.

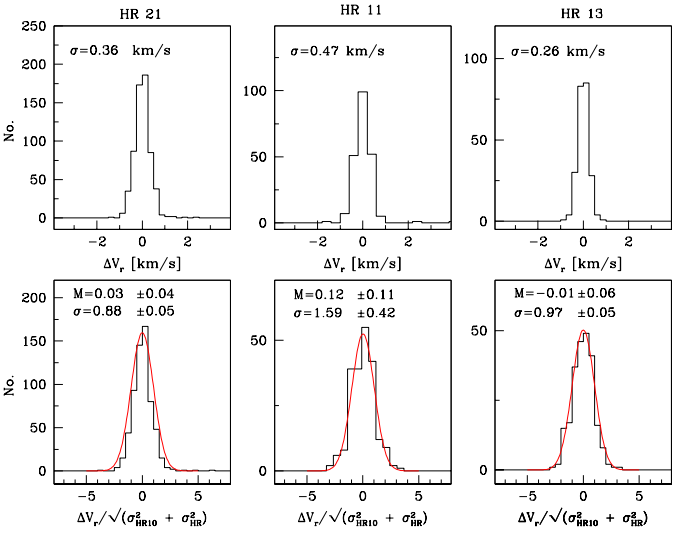

Fig. 5. Comparison between velocity measurements for stars observed in two Giraffe setups. *Upper panels*: we show the distribution of velocity differences with respect to the velocity measured with HR 10 for all the stars observed (from left to right, with HR 21, HR 11 and HR 13) and estimated uncertainties on $V_r \leq 1$ km s^{-1} for each measurement. The mean difference and the *rms* dispersion are also shown. *Bottom panels*: as above, but now the velocity difference is normalised by the predicted uncertainty. It can be appreciated that the measured uncertainty in the velocity distribution is very close to the unit variance Gaussian (standard deviation = 0.88, 1.59, and 0.97 for HR 21, HR 11, and HR 13, respectively).

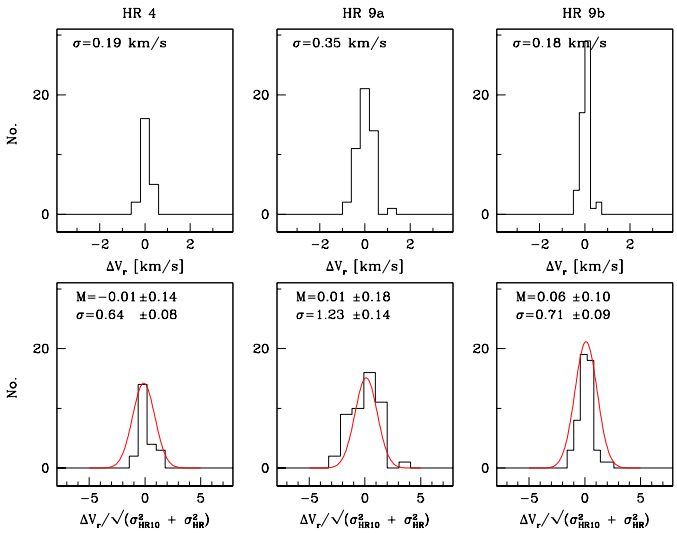

Fig. 6. Same as Fig. 5, but for HR 4, HR 9A, and HR 9B.

0.06, σ = 0.7 km s^{-1}). For NGC 5927 we measured a mean difference of V_r(this paper)- V_r(Simmerer)= –0.03, σ=0.41 km s^{-1} for the stars in common with the sample presented in Simmerer et al. (2013).

2.3. V_r errors from repeated measurements

We tested the reliability of the pipeline-delivered V_r and their associated uncertainties by analysing the distribution of velocity differences from repeated measurements. We assumed that the nth observed velocity v_n (i.e., in different GIRAFFE setups) can be considered a random variable that follows a Gaussian distribution centred on the true velocity value V_r and with dispersion given by the velocity uncertainty σ_n. The difference between two repeated, independent measurements v_1 and v_2 , $\Delta v = v_1 - v_2$, is a random variable following a Gaussian distribution centred on zero and with a dispersion given by $\sigma = \sqrt{\sigma_1^2 + \sigma_2^2}$. If both velocity and the related uncertainties are well determined, the distribution of velocity differences Δv normalised by σ should be a Gaussian with mean zero and dispersion unity. We considered all stars observed at least in two setups (i.e., HR 10 and another GIRAFFE setup) and plotted the velocity differences and the normalised velocity differences for all the considered clusters[5]. Figure 5 shows that if we take into consideration all stars observed with HR 21, HR 11, and HR 13 (i.e., the setups for which we have the largest number of spectra available), all clusters have distributions with Gaussian appearance and dispersion equal to (or lower than) unity. We found that normalised Δv distributions are all close to Gaussian, with a resulting standard deviation always smaller than 1.6, but typically equal to or lower than unity for the remaining setups[6] (see Figs. 5, 6, and 7). We found higher σ values for the setups that are commonly used for hot or rotating horizontal branch stars.

[5] Each velocity estimate was previously corrected for the shifts listed in Table 2.

[6] We do not plot the comparison between velocity measurements for stars observed in both HR 10 and HR 19A because there are only two stars in common between these two setups.

Table 2. The sample and its internal V_r accuracy

Cluster	$\langle\Delta V_r\rangle^{HR10-HR21}$ (km s^{-1})	$\langle\Delta V_r\rangle^{HR10-HR11}$ (km s^{-1})	$\langle\Delta V_r\rangle^{HR10-HR13}$ (km s^{-1})	$\langle\Delta V_r\rangle^{HR10-HR4}$ (km s^{-1})	$\langle\Delta V_r\rangle^{HR10-HR9A}$ (km s^{-1})
M 15	–0.83 (σ = 0.27, 78)	–0.36 (σ = 0.30, 12)	–0.10 (σ = 0.24, 26)		
NGC 4372	–0.99 (σ = 0.32, 100)		–0.19 (σ = 0.24, 42)		
NGC 4833	–0.69 (σ = 0.37, 77)	0.29 (σ = 1.61, 8)	–0.02 (σ = 0.66, 8)		
NGC 6752	–1.00 (σ = 0.33, 108)	–0.58 (σ = 0.34, 148)	–0.20 (σ = 0.22, 105)	0.118 (σ =0.190, 23)	
NGC 1851	–0.94 (σ = 0.39, 91)	–0.30 (σ = 0.25, 51)	–0.67 (σ = 0.31, 56)		0.15 (σ = 0.35, 52)
NGC 2808	–0.63 (σ = 0.32, 58)		0.07 (σ = 0.02, 2)		
NGC 5927	–0.56 (σ = 0.21, 108)				

Cluster	$\langle\Delta V_r\rangle^{HR10-HR9B}$ (km s^{-1})	$\langle\Delta V_r\rangle^{HR10-HR14A}$ (km s^{-1})	$\langle\Delta V_r\rangle^{HR10-HR14B}$ (km s^{-1})	$\langle\Delta V_r\rangle^{HR10-HR15N}$ (km s^{-1})	$\langle\Delta V_r\rangle^{HR10-HR19A}$ (km s^{-1})
M 15		–0.25 (σ = 0.95, 12)			
NGC 4372		–0.62 (σ = 0.48, 22)			
NGC 4833					
NGC 6752	–0.29 (σ = 0.15, 51)		–0.54 (σ = 0.23, 54)	–1.39 (σ = 0.37, 25)	
NGC 1851					–0.232 (σ = 0.005, 2)
NGC 2808		–0.175 (σ = 0.01, 2)			
NGC 5927					

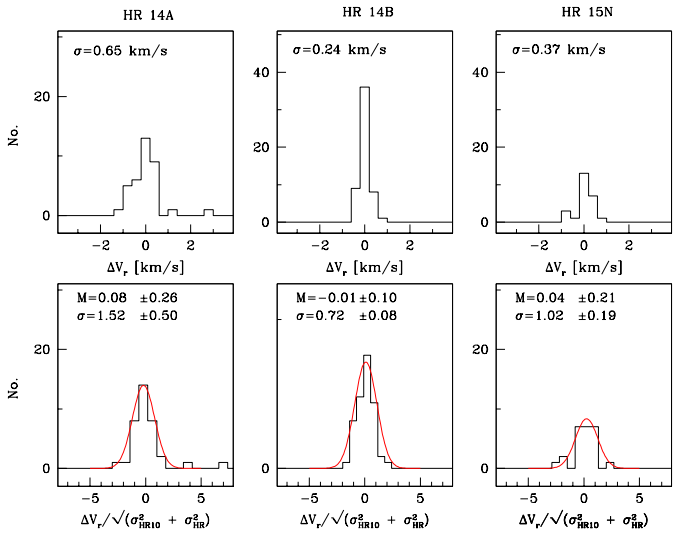

Fig. 7. Same as Fig. 5, but for HR 14A, HR 14B, and HR 15N.

2.4. Membership

The distribution of the radial velocity of all the observed stars as a function of their (projected) distance from the centre is shown in Fig. 8. The coordinates of the cluster centre are taken from Shawl & White (1986) for NGC 4372 and NGC 4833, Goldsbury et al. (2010) for NGC 5927, and Noyola & Gebhardt (2006) for the remaining clusters. The distribution of radial velocities for the cluster members can be easily isolated from field contaminants in almost all cases. Therefore, as a first broad selection, we kept as cluster members all stars with V_r between the two dashed lines in Fig. 8. We then computed the mean and dispersion of this sample and retained all stars with V_r within $\pm 3\sigma$ range around the global mean (i.e., stars enclosed within the two dotted lines in the same figure).

Kouwenhoven & de Grijs (2008) demonstrated that even a binary fraction as high as 100 percent could lead to an increase in the observed velocity dispersion to lower than ≤ 0.5 km s^{-1}. Since GCs have typical binary fractions ≤ 20 percent (i.e., Sollima et al. 2007 and Milone et al. 2008), we considered binaries as a negligible factor for our analysis. We expect some (limited) contamination from Milky Way stars, even in our V_r -selected sample. We used the Besançon model (Robin et al. 2003) to simulate a set of V_r for stars that correspond to the direction, colour, and magnitude survey of the targets. The Besançon model suggests that some spurious Milky Way contaminant may be present even in the relatively narrow V_r range we have adopted to select stars. In the right-hand panel of Fig. 8, we show the histograms of the distribution of the V_r for each cluster, the number of stars selected as possible cluster members, and the (small percent) contamination expected according to Robin et al. (2003) Galactic model. Finally, in the following sections, we reconsider individual memberships based on the velocity distributions as a function of distance from the cluster centre.

3. Velocity dispersion profiles

Although all clusters we studied have kinematic data already available in the literature (for an update summary we refer to Table 1 of B12), there are a few clusters for which we can provide a significant improvement over existing kinematic data and analyses. For example, while M 15 has been extensively studied (van den Bosch et al. 2006 presented a detailed analysis of this cluster based on nearly two thousand V_r and proper motions), for NGC 5927 no velocity dispersion profile and no estimate of the central velocity dispersion are available in the literature (Simmerer et al. 2013 provided only an estimate of the overall dispersion). For several clusters the samples presented in the literature are smaller than (NGC 6752, NGC 1851; Lane et al. 2010b; Scarpa et al. 2011; Carretta et al. 2010, 2011) or similar to (NGC 4833, NGC 4372; Carretta et al. 2014; Kacharov et al. 2014) those considered here. An independent check of the results from previous analyses is provided. In the following we briefly discuss the properties of the V_r distributions and derive new estimates of the central velocity dispersion (σ_0) in all the selected clusters.

We used radial velocities of member stars to produce velocity dispersion (σ) curves for all the considered clusters as described in Bellazzini et al. (2008), using *jackknife* resampling (Lupton 1993) to compute uncertainties. In the upper panel of Figs. 9 to 15 we show the V_r distribution as a function of R (distance from the centre). We divided the whole sample into several independent radial bins of different size, manually cho-

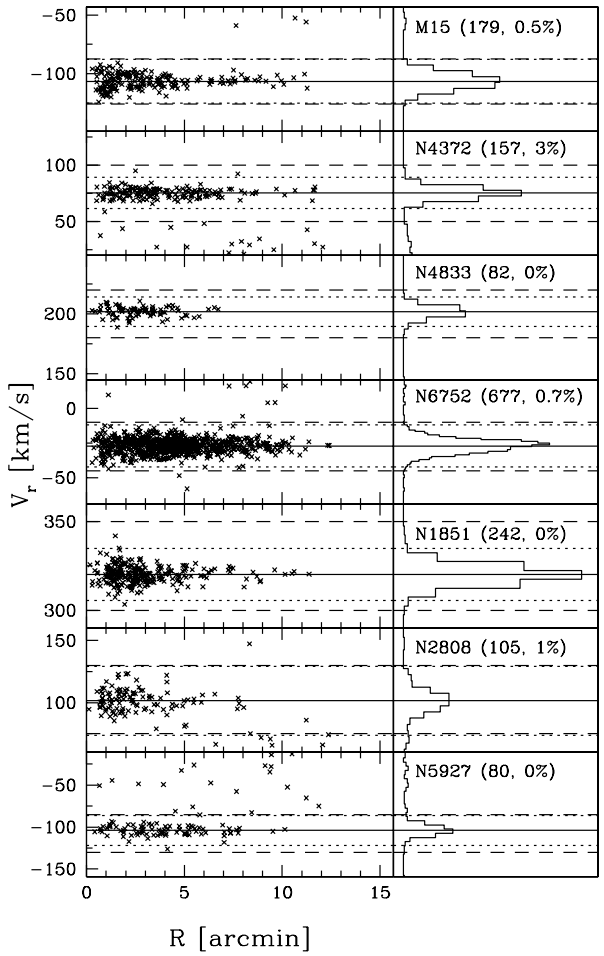

Fig. 8. Radial velocity of program stars as a function of distance from the center (*left-hand panel*) for all the considered clusters, and radial velocity distribution (*right-hand panel*). The long-dashed lines mark the range we adopted for the first selection of candidate cluster members. The dotted lines enclose the (global) $\pm 3\sigma$ range from the mean of the selected samples of candidates (continuous line), their number size is also indicated in the right-hand panel, along with the percentage of expected contaminants from the Besançon models (see text).

sen as a compromise between maintaining the highest degree of spatial resolution while considering a statistically significant number ($\simeq$ 15) of stars. In each bin we computed the average V_r - $\langle V_{sys} \rangle$ and velocity dispersion σ, with their uncertainties. An iterative 3σ clipping algorithm was applied bin by bin. Any star rejected by the clipping algorithm was then rejected from the following analysis. The rejected stars are indicated in the plots as crosses. The V_r estimates for all the stars judged to be members are reported in Table 3, together with other stellar parameters. In Table 4 we report the measured average velocity for each cluster. From this table we note an excellent agreement between the cluster average velocity derived here and those reported in literature.

The derived velocity dispersion profile is reported in the lower panel of the figures and listed in Table 5. The profiles are complemented with the central estimate obtained from the literature (large empty pentagon in the same figures).

We fitted the resulting velocity dispersion profile in a least-squares sense with the predictions of the King (1966) (hereafter

Table 3. Radial velocities for the stars.

NGC	ID	RA (deg)	Dec (deg)	V (mag)	V_r km s^{-1}	eV_r km s^{-1}
7078	1	322.4817397	12.1793098	12.8	-118.90	0.64
7078	2	322.5093355	12.1893088	12.8	-98.25	0.24
7078	3	322.5037366	12.1491900	12.9	-114.20	0.38
7078	4	322.5013943	12.1808019	13.0	-116.60	0.41
7078	5	322.4908124	12.1577422	13.2	-95.12	0.24
7078	6	322.4993224	12.1571307	13.3	-112.00	0.11

Notes. A portion of the table is shown for guidance about its content, the complete table is available in electronic format through the CDS service.

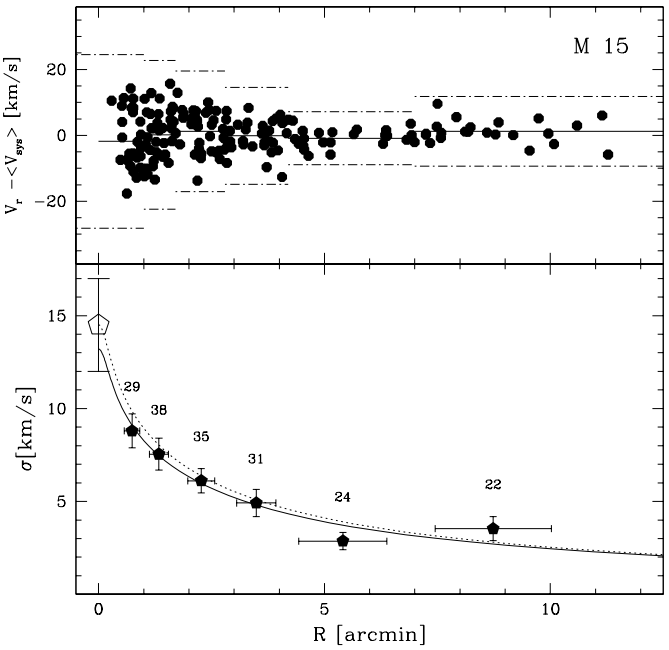

Fig. 9. Velocity dispersion profile of M 15 stars. The upper panel shows the V_r distribution as a function of distance from the cluster centre for individual stars of the sample. Only stars plotted as dots are retained to compute σ in the various radial bins: crosses are stars rejected only because they are *local* 3σ outliers of the bins. The mean V_r - $\langle V_{sys} \rangle$ is marked by the continuous horizontal line. Comparison of the observed velocity dispersion profile of M15 with the King model with a core radius r_C= 0.07′and a concentration C=2.5, from Trager et al. (1993) and normalised to σ_0=13.2 km s^{-1} (continuous line; our estimate) and σ_0=14.5 km s^{-1} (dotted line; by McNamara et al. 2003). The large filled pentagons are the dispersions estimated in the corresponding bins displayed in the upper panel, with their bootstrapped errors. The number of stars per bin is also reported above the points. The open pentagon is the value of σ at the centre of M 15 from McNamara et al. (2003).

K66) model that best fits the surface brightness profile (according to Trager et al. 1993), leaving the central velocity dispersion $\sigma_0$as the free parameter to be determined. It is important to note that our σ_0 estimates are extrapolations to r=0 of the isotropic single-mass K66 model that best fits the observed velocity dispersion profile. Hence they are model-dependent and based on models that are known not to be perfectly adequate to describe real clusters, which, for instance, are populated by stars of different masses. The reliability of each estimate of σ_0 depends on

the radial coverage of the velocity dispersion profile and on the cluster surface brightness profile; it can be judged relatively easily from inspecting Figs. 7-13 below.

In general, our V_r^{sys} and the σ_0 estimates agree well with those found in previous studies (see Table 4), except for two cases.

For NGC 6752 we estimated a velocity dispersion toward the centre of σ_0 = 8.2 km s^{-1}, which is higher than that found by Lane et al. (2010b) (σ_0 = 5.7 ± 0.7 km s^{-1})[7]. This can be partially due to the fact that they estimated σ_0 by extrapolating from a different class of models than we did here, that is, Plummer (1911) instead of K66. Our observed velocity dispersion profile is fully compatible with that by Lane et al. (2010b) in the wide range where the two profiles overlaps. The inspection of the two curves suggests that the true value of σ_0 can be in between the two estimates. On the other hand, the two estimates based on radial velocities are significantly lower than the one consistently derived from the two components of the proper motions in the plane of the sky by Drukier et al. (2003) (σ_0 = 12.4 ± 0.5 km s^{-1}; see Fig. 10). This large discrepancy with the Drukier et al. (2003) *measured* value can be due to the adoption of a cluster distance that overestimates the true value, to a significantly different mean mass of the adopted tracers (e.g., giants vs. subgiants+dwarfs), or to a significant amount of orbital anisotropy (see Drukier et al. 2003). In any case, our data provide the final proof that the discrepancy between the dispersion from radial velocity and from proper motions, already noted by Drukier et al. (2003) is real and requires further investigation.

For NGC 2808, the sparse dispersion profile we obtained provides only weak constraints on σ_0, hence the difference between our extrapolated value and the value listed in Pryor & Meylan (1993) cannot be considered significant. We recall that the latter is from an integrated spectrum taken at the cluster centre, and it fully agrees with the recent measurement by Lützgendorf et al. (2012).

For NGC 5927 we present for the first time a velocity dispersion profile in Fig. 15. We also provide the first estimate of σ_0, but we note that the constraint on this parameter provided by our profile is relatively weak, hence the associated uncertainty is quite large (of about 2 km s^{-1}).

4. Rotation

We used our sample to search for a rotation signal in all the considered clusters. To do this, we used the same method as adopted by Cote et al. (1995), Pancino et al. (2007), Lane et al. (2009, 2010a,b), and B12. Rotations were measured by halving the cluster by position angle (PA)[8] and calculating the mean radial velocity of each half. This was performed in steps of 20-35° depending on the number of the observed stars in the considered cluster to avoid aliasing effects. The two mean velocities were then subtracted, and the difference in the mean V_r for each PA of the dividing line is plotted in Fig. 16 as a function of the PA and the best-fitting sine function

$$\Delta\langle V_r\rangle = A_{\rm rot}\sin(PA + \Phi),$$

where $\Phi = 270° - PA_0$, PA_0 is the position angle of the dividing line corresponding to the maximum rotation amplitude (degrees), and A_{rot} is twice the actual mean amplitude (in km s^{-1}; see Lane et al. 2010a and B12). $A_{rot}/2$ should be considered as an underestimate of the maximum projected rotational ampli-

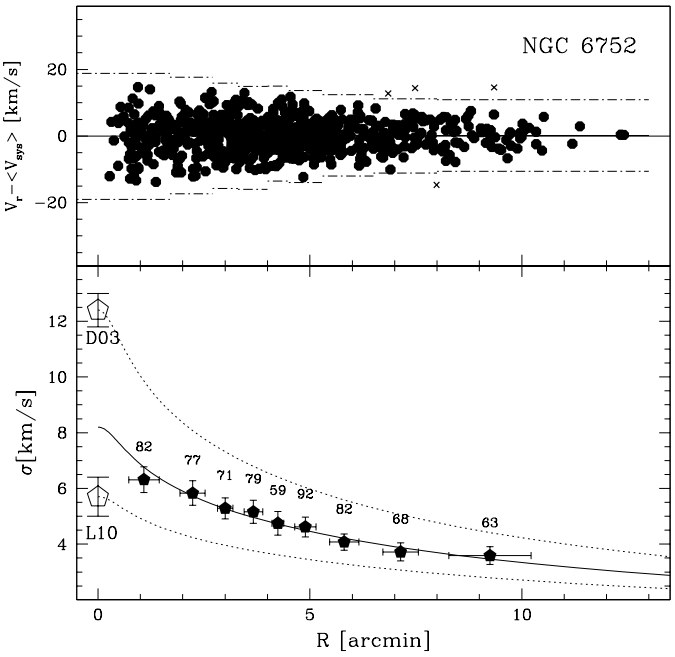

Fig. 10. Same as in Fig. 9, but for NGC 6752. Core radius (r_C= 0.17′) and concentration (C=2.5) are from Trager et al. (1993) and K66 models are normalised to σ_0=8.2 km s^{-1} (continuous line; our estimate) and σ_0=5.7 and 12.4 km s^{-1} (dotted lines; by Lane et al. 2010b (L10) and Drukier et al. 2003 (D03)). The large open pentagons are the values of σ at the centre from L10 and D03.

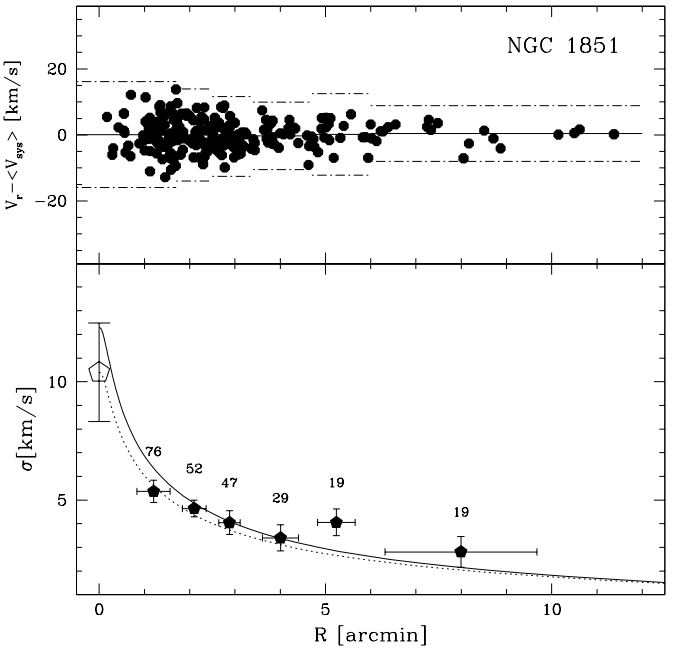

Fig. 11. Same as in Fig. 9, but for NGC 1851. Core radius (r_C=0.08′) and concentration (C=2.24) are from Trager et al. (1993) and K66 models are normalised to σ_0=12.3 km s^{-1} (continuous line; our estimate) and σ_0=10.4 km s^{-1} (dotted line; by Pryor & Meylan 1993). The open pentagon is the value of σ at the centre from Pryor & Meylan (1993).

[7] For reference Dubath et al. (1997) obtained σ_0 = 4.9 ± 2.4 km s^{-1} from integrated-light spectra.

[8] In the adopted approach PA is defined to increase anti-clockwise in the plane of the sky from north (PA = 0°) toward east (PA = 90°).

Table 4. Comparison between the systemic radial velocities derived in this paper with literature values.

Target	V_r (t.p.) km s^{-1}	dispersion (t.p.) km s^{-1}	V_r (lit.) km s^{-1}	dispersion (lit.) km s^{-1}	References
M 15	–106.4±0.7	6.2	–106.7±0.4	11.8	McNamara et al. (2003)
NGC 1851	320.1±0.3	4.4	320.3±0.4	3.7	Carretta et al. (2010)
NGC 2808	101.4±1.0	9.5	102.4±0.9	9.8	Carretta et al. (2006)
NGC 4372	75.2±0.4	3.9	75.9±0.4	3.8	Kacharov et al. (2014)
NGC 4833	202.1±0.6	3.9	202.0±0.5	4.1	Carretta et al. (2014)
NGC 5927	–103.95±0.7	5.1	–104.0±0.6	5.0	Simmerer et al. (2013)
NGC 6752	–26.9±0.2	5.0	–26.1±0.2	4.7	Lane et al. (2010b)

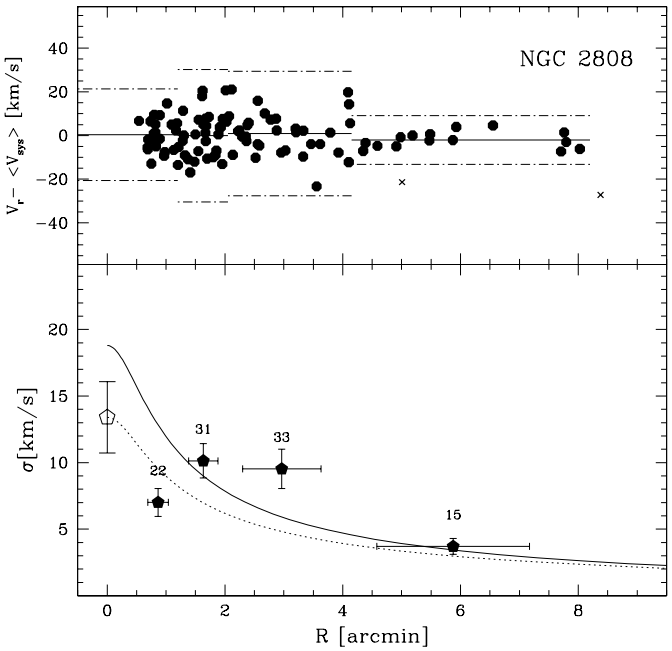

Fig. 12. Same as in Fig. 9, but for NGC 2808. Core radius (r_C=0.26′) and concentration (C=1.8) are from Trager et al. (1993) and K66 models are normalised to σ_0=18.8 km s^{-1} (continuous line; our estimate) and σ_0=13.4 km s^{-1} (dotted line; by Pryor & Meylan 1993). The open pentagon is the value of σ at the centre from Pryor & Meylan (1993).

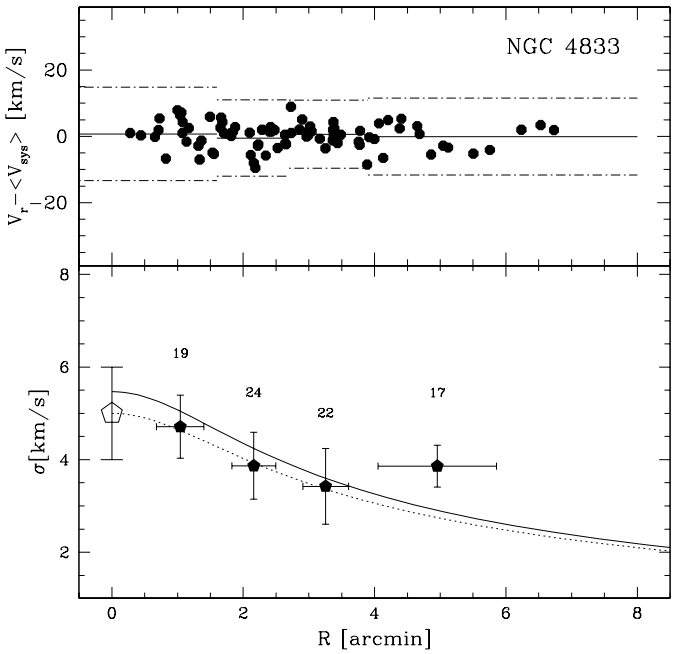

Fig. 13. Same as in Fig. 9, but for NGC 4833. Core radius (r_C=1.0′) and concentration (C=1.25) are from Trager et al. (1993) and K66 models are normalised to σ_0=5.5 km s^{-1} (continuous line; our estimate) and σ_0=5.0 km s^{-1} (dotted line; by Carretta et al. 2014). The open pentagon is the value of σ at the centre from Carretta et al. (2014).

tude because the $\langle V_r \rangle$ difference is actually averaged over the full range of radial distances covered by the targeted stars, and the amplitude does vary with distance from the cluster centre (Sollima et al. 2009). But even if the derived A_{rot} are only estimates of the amplitude of the projected rotation pattern, we can consider A_{rot} as a proxy for the true amplitude, in a statistical sense (see Appendix A in B12). The estimates of A_{rot} should be considered as quite robust. We measured a typical 1σ uncertainty ranging from 0.15 km s^{-1} in the case of M 15, to 0.8 km s^{-1} for NGC 5927. On the contrary, PA_0 is more sensitive to the spatial distribution of the adopted sample, with an associated uncertainty at the ± 30° level in the best cases.

The considered clusters span a wide range of rotation amplitude, from no rotation within the uncertainties (NGC 6752) to an amplitude of more than 3.5 km s^{-1} (NGC 2808 and M 15). We note that the two clusters with clear rotation pattern, NGC 2808 and M 15, are among the most peculiar clusters in terms of multiple populations, with an extended horizontal branch morphology (see for a recent review Gratton et al. 2012 and references therein). For the six clusters already considered in previous studies (i.e., all the sample clusters but NGC 5927), we confirm the results reported in the literature, while we were able to detect for the first time a significant amplitude of rotation for the metal-rich cluster[9] NGC 5927, A_{rot} = 2.6 km s^{-1}.

In Fig. 17 we show the rotation curves for M 15, NGC 1851, NGC 2808, and NGC 5927; these are the four clusters for which significant rotation was detected. In the right-hand panels, the V_r distribution of stars lying on opposite sides with respect to the rotation axis are compared. If the clusters were non-rotating, the two distributions would be identical, while a shift should be apparent with significant rotation [10]. A Kolgomorov-Smirnov test shows instead that it is relatively unlikely that the observed patterns may emerge by chance from non-rotating systems (see left-hand panels of Fig. 17).

[9] The value tabulated in the Harris 1996 catalogue for NGC 5927 is [Fe/H]= –0.49 dex; it was obtained by averaging the [Fe/H] derived by Armandroff & Zinn 1988; Francois 1991; Carretta et al. 2009a.

[10] We note that the degree to which the two distributions differ also depends on the ratio between rotation and velocity dispersion and on the actual shape of the rotation curve.

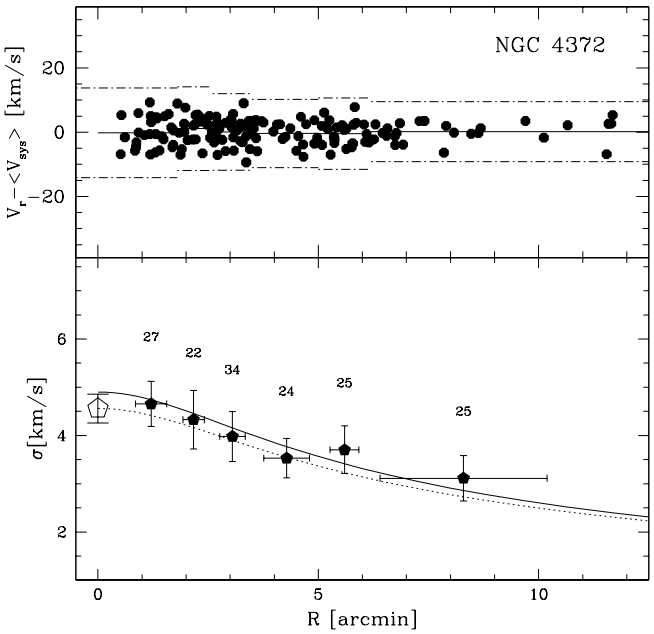

Fig. 14. Same as in Fig. 9, but for NGC 4372. Core radius (r_C=1.74′) and concentration (C=1.30) are from Trager et al. (1993) and K66 models are normalised to σ_0=4.9 km s^{-1} (continuous line; our estimate) and σ_0=4.56 km s^{-1} (dotted line; by Kacharov et al. 2014). The open pentagon is the estimate of σ at the centre from Kacharov et al. (2014) based on the fit of a Plummer profile and a rotating, physical model.

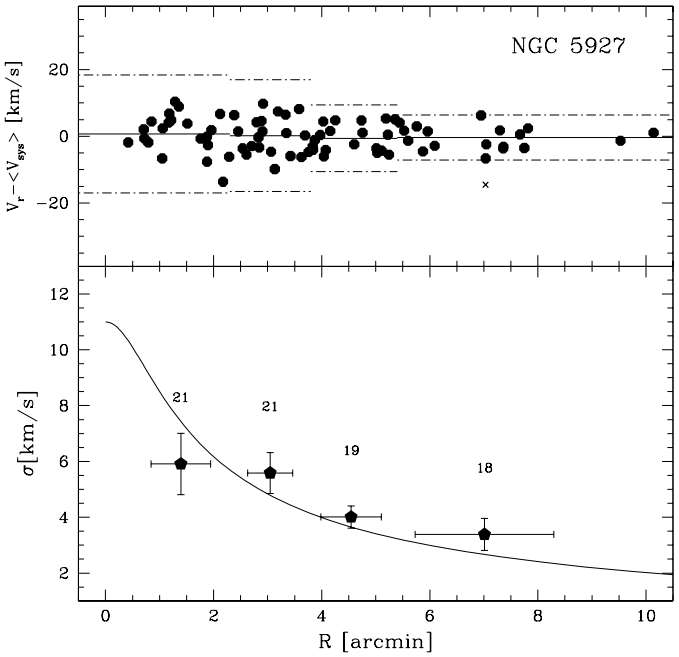

Fig. 15. Same as in Fig. 9, but for NGC 5927. Core radius (r_C=1.40′) and concentration (C=1.60) are from Trager et al. (1993) and K66 models are normalised to σ_0=11.0 km s^{-1} (continuous line; our estimate).

5. Trends with cluster parameters

B12 used kinematic data for several GCs to explore the dependences of several GC parameters on the A_{rot} and A_{rot}/σ_0. In particular, these authors made use of the large database (≃ 2000 stars) collected in the framework of the Na-O anti-correlation and HB program (see for example Carretta et al. 2009b,c for a more detailed description). The B12 database included 24 GCs that partially overlap with our sample (see also Meylan & Heggie 1997), and our study is largely homogeneous with their analysis. Therefore, we added three new clusters to the compilation in B12 (i.e., NGC 4372, NGC 4833, and NGC 5927) and considered for the clusters in common our own values of the central velocity dispersion and A_{rot}.

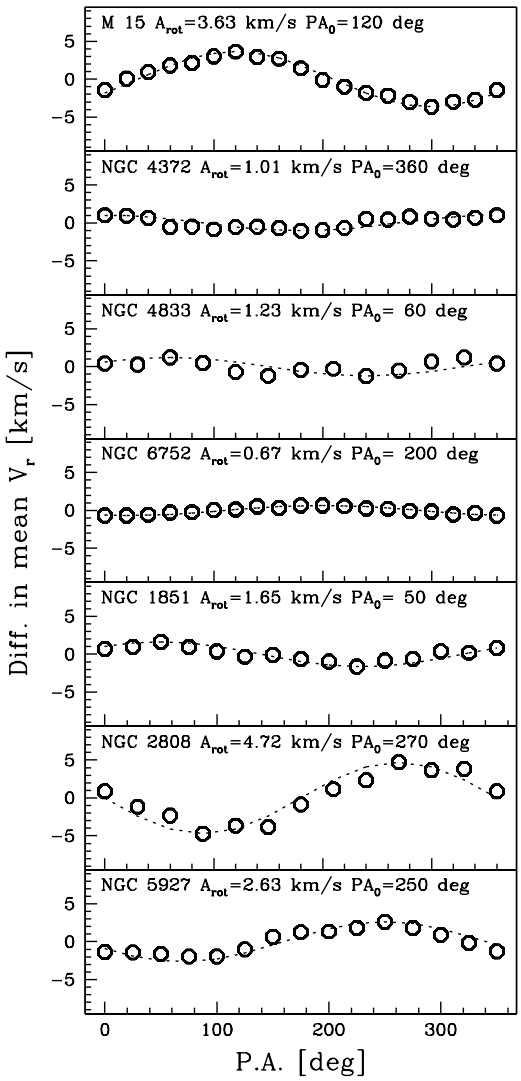
M 15 A_{rot}=3.63 km/s PA_0=120 deg
NGC 4372 A_{rot}=1.01 km/s PA_0=360 deg
NGC 4833 A_{rot}=1.23 km/s PA_0= 60 deg
NGC 6752 A_{rot}=0.67 km/s PA_0= 200 deg
NGC 1851 A_{rot}=1.65 km/s PA_0= 50 deg
NGC 2808 A_{rot}=4.72 km/s PA_0=270 deg
NGC 5927 A_{rot}=2.63 km/s PA_0=250 deg
Diff. in mean V_r [km/s]
P.A. [deg]

Fig. 16. Rotation in our program GCs. The plots display the difference between the mean velocities of each side of a cluster with respect to a line passing through the cluster centre with a varying PA (measured from north to east), as a function of the adopted PA. The dashed line is the sine law that best fits the observed pattern. The rotational amplitude (A_{rot}) and the position angle (PA) are also indicated.

Table 5 lists σ_0 and A_{rot} estimates for all the clusters, together with other relevant parameters from various sources. In Fig. 18 we show the behaviour of the ratio A_{rot}/σ_0 as a function of metallicity, the HB morphology parameter HBR = (B – R)/(B + V + R) (Lee 1990, see caption in Table 5 for its definition), the absolute integrated V magnitude (M_V), the logarithm of the central luminosity density (log ρ_0), and the distance from the Galactic centre (R_{GC}). The same figure also reports the Pearson (r_P) and Spearman (r_S) correlation coefficients. The ratio A_{rot}/σ_0

Table 5. Cluster parameters

Cluster	σ_0 km s^{-1}	ϵ_σ km s^{-1}	A_{rot} km s^{-1}	ϵ_A km s^{-1}	[Fe/H] dex	HBR	M_V	ell	log ρ_0 $L_\odot$ pc^{-3}	R_G kpc
NGC 104	9.6	0.6	4.4	0.4	-0.76	-0.99	-9.42	0.09	4.88	7.4
NGC 288	2.7	0.8	0.5	0.3	-1.32	0.98	-6.75	0.00	1.78	12.0
NGC 1851	12.3[a]	1.5	1.6[a]	0.5	-1.16	-0.32	-8.33	0.05	5.09	16.6
NGC 1904	5.3	0.4	0.6	0.5	-1.58	0.89	-7.86	0.01	4.08	18.8
NGC 2808	18.8[a]	4.0	4.7[a]	0.2	-1.18	-0.49	-9.39	0.12	4.66	11.1
NGC 3201	4.5	0.5	1.2	0.3	-1.51	0.08	-7.45	0.12	2.71	8.8
NGC 4372	4.9[a]	1.2	1.0[a]	0.5	-2.17[b]	1.00[c]	-7.77[c]	0.15[c]	2.06[b]	7.1[c]
NGC 4590	2.4	0.9	1.2	0.4	-2.27	0.17	-7.37	0.05	2.57	10.2
NGC 4833	5.5[a]	1.5	1.2[a]	0.4	-1.85[b]	0.93[c]	-8.16[c]	0.07[c]	3.00[b]	7.0[c]
NGC 5024	4.4	0.9	0.0	0.5	-2.06	0.81	-8.71	0.01	3.07	18.4
NGC 5139	19.0	1.0	6.0	1.0	-1.64	-	-10.26	0.17	3.15	6.4
NGC 5904	7.5	1.0	2.6	0.5	-1.33	0.31	-8.81	0.14	3.88	6.2
NGC 5927	11.0[a]	2.0	2.6[a]	0.8	-0.49[b]	-1.00[c]	-7.80[c]	0.04[c]	4.09[b]	7.3[c]
NGC 6121	3.9	0.7	1.8	0.2	-1.18	-0.06	-7.19	0.00	3.64	5.9
NGC 6171	4.1	0.3	2.9	1.0	-1.03	-0.73	-7.12	0.02	3.08	3.3
NGC 6218	4.7	0.9	0.3	0.2	-1.33	0.97	-7.31	0.04	3.23	4.5
NGC 6254	6.6	0.8	0.4	0.5	-1.57	0.98	-7.48	0.00	3.54	4.6
NGC 6388	18.9	0.8	3.9	1.0	-0.45	-0.65	-9.41	0.01	5.37	3.1
NGC 6397	4.5	0.6	0.2	0.5	-1.99	0.98	-6.64	0.07	5.76	6.0
NGC 6441	18.0	0.2	12.9	2.0	-0.44	-0.76	-9.63	0.02	5.26	3.9
NGC 6656	6.8	0.6	1.5	0.4	-1.70	0.91	-8.50	0.14	3.63	4.9
NGC 6715	16.4	0.4	2.0	0.5	-1.56	0.54	-9.98	0.06	4.69	18.9
NGC 6752	8.2[a]	0.6	0.7[a]	0.2	-1.55	1.00	-7.73	0.04	5.04	5.2
NGC 6809	2.7	0.5	0.5	0.2	-1.93	0.87	-7.57	0.02	2.22	3.9
NGC 6838	2.3	0.2	1.3	0.5	-0.82	-1.00	-5.61	0.00	2.83	6.7
NGC 7078	13.2[a]	1.5	3.6[a]	0.1	-2.33	0.67	-9.19	0.05	5.05	10.4
NGC 7099	5.0	0.9	0.0	0.0	-2.33	0.89	-7.45	0.01	5.01	7.1

Notes. All parameters are reported from Bellazzini et al. (2012) except:
[(a)] this work
[(b)] Harris 1996 (2010 edition)
[(c)] Mackey & van den Bergh (2005)
Meaning of columns:
(1) Cluster name; (2) central radial velocity dispersion; (3) error on σ_0; (4) projected rotation amplitude; (5) error on A_{rot}; (6) mean iron abundance ratio; (7) HB morphology, where HBR = (B – R)/(B + V + R), where B is the number of stars bluer than the instability strip, R redder, and V the number of variables in the strip; (8) the integrated V magnitude; (9) the isophotal ellipticity $\epsilon = 1 - (b/a)$; (10) central luminosity density; (11) distance from the Galactic centre (kpc).

does not show any clear correlation with M_V, ellipticity, log ρ_0, and R_{GC}. On the contrary, a clear correlation emerges between A_{rot}/σ_0 with [Fe/H] and HBR (see B12). For more metal-rich clusters the relevance of ordered motions with respect to pressure is stronger. According to a two-tailed Student's test, the probability that a Spearman rank correlation coefficient equal to or higher than the observed one ($r_S = 0.423$) is produced by chance from uncorrelated quantities is $P_t = 3.0\%$ (27 clusters), so the correlation can be considered as statistically significant. In addition, the A_{rot}/σ_0 ratio appears to be significantly correlated with the HB morphology ($P_t = 1 \times 10^{-4}$) in the sense that clusters with redder HB have greater fractions of ordered motions with respect to pressure support.

Additionally, Fig. 19 shows that A_{rot} has statistically significant correlation with HBR ($P_t = 1 \times 10^{-5}$), M_V ($P_t = 5 \times 10^{-4}$), σ_0($P_t = 2 \times 10^{-4}$), and [Fe/H] ($P_t = 4 \times 10^{-3}$)[11]. All the above results agree well with those reported by B12.

[11] We caution, however, that the statistics quoted for P_t could be slightly misleading because a correlation may emerge even in a random dataset, whereas there are enough parameters and enough correlation plots.

6. Summary and conclusions

We used the radial velocity estimates obtained from the second internal data release of data products to ESO of the Gaia-ESO survey to study the kinematics of seven Galactic GCs. We confirm the central velocity estimates reported in the literature for NGC 1851, M 15, NGC 4372, and NGC 4833, while we found that there is a real discrepancy between the central dispersion from radial velocities and that from proper motions for NGC 6752. For NGC 2808, our sample is too sparse to draw useful conclusions about σ_0. Finally, we provided for the first time a velocity dispersion profile and a central velocity dispersion estimate for NGC 5927, albeit uncertain (see Sect. 3). We searched for systemic rotation in all the studied clusters and found significant rotation patterns ($A_{rot} \geq 2.5$ km s^{-1}) in NGC 2808, NGC 5927, and M 15 and a marginal detection for NGC 1851 (see Sect. 4).

We demonstrated that the radial velocities delivered from the Gaia-ESO survey pipeline have sufficient quality to be used in a profitable way in a kinematic study and made public a large database of radial velocities of GCs members for future research. For example, we verified that the uncertainties on individual radial velocity estimates from the survey pipeline are fully reliable because they match the errors on the mean derived from multiple independent measures.

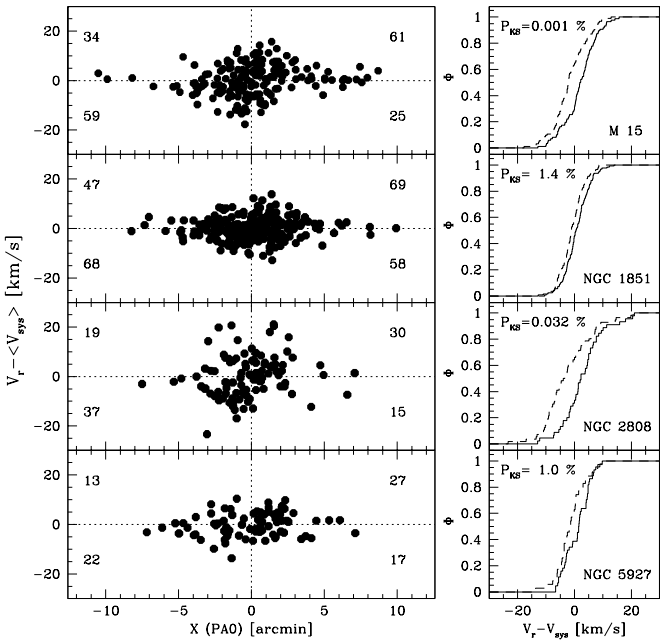

Fig. 17. Rotation curves for M 15, NGC 1851, NGC 2808, and NGC 5927. *Left panels*: V_r in the system of the cluster as a function of distance from the centre projected onto the axis perpendicular to the best-fit rotation axis found in Fig. 16. The number of stars in each quadrant is also shown. *Right panels*: comparison of the cumulative V_r distributions of stars with X(PA0) > 0.0 (continuous lines) and X(PA0) < 0.0 (dashed lines). The probability that the two distributions are drawn from the same parent population (according to a KS test) is reported in each panel. We show rotation curves only for the four clusters with $P_{KS} < 2.5\%$.

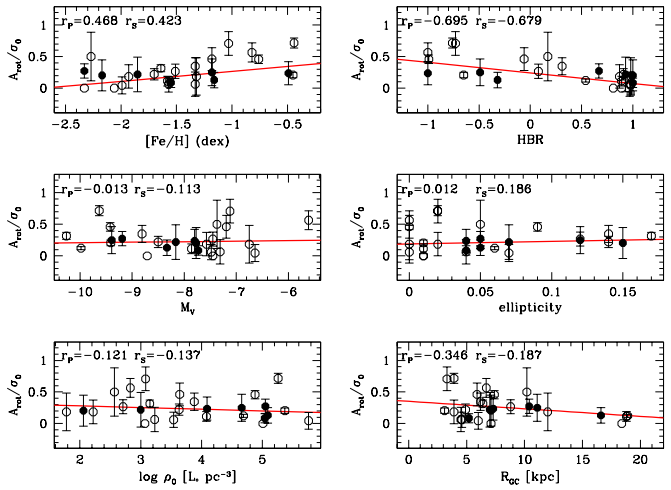

Fig. 18. Ratio between the amplitude of the rotation A_{rot} and the central velocity dispersion σ_0 versus various other parameters. Red lines mark weighted linear fits to the clusters, and the correlation coefficients are reported at the top of each panel: r_S stands for the Spearman and r_P for the Pearson coefficient. Empty circles are data from B12, while filled circles are our own estimates.

When all the archival data will be incorporated into the Gaia-ESO survey and abundances will be available for all the analysed stars, the final large dataset will permit insightful analyses of the internal motions of the clusters. For example, it will allow us to correlate the presence and amplitude of rotation with the

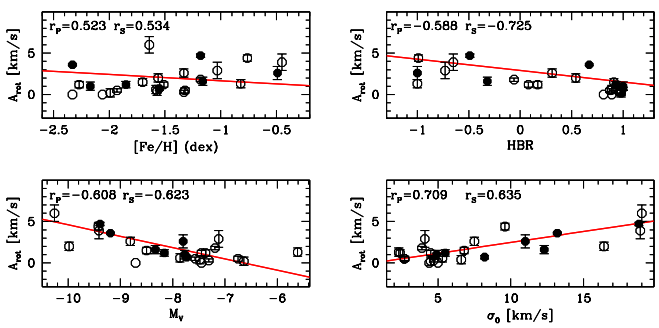

Fig. 19. Run of the amplitude of the rotation A_{rot} vs. versus various other parameters. Red lines mark weighted linear fits to the clusters (filled and empty) and the correlation coefficients are reported at the top of each panel: r_S stands for the Spearman and r_P for the Pearson coefficient. Empty circles are from B12, while filled circles are our own estimates.

cluster parameters, different chemistry and/or sub-population. Moreover, the Gaia satellite will provide 3D kinematical data for a significant number of these stars (see Pancino et al. 2013), so that the analysis we presented here can be considered as a preparatory study aimed at a complete exploitation of the Gaia data.

Acknowledgements. We thank the referee, N. Martin, for the careful reading of the manuscript and for the useful comments and suggestions that helped to improve the quality of the paper significantly. We acknowledge the support from INAF and Ministero dell' Istruzione, dell' Università e della Ricerca (MIUR) in the form of the grants "Premiale VLT 2012" and "The Chemical and Dynamical Evolution of the Milky Way and Local Group Galaxies" (prot. 2010LY5N2T). PdL and ARB acknowledge the support of French Agence Nationale de la Recherche, under contract ANR-2010-BLAN-0508-01OTP, and the Programme National de Cosmologie et Galaxies. This work was partly supported by the European Union FP7 programme through ERC grant number 320360 and by the Leverhulme Trust through grant RPG-2012-541. The results presented here benefit from discussions held during the Gaia-ESO workshops and conferences supported by the ESF (European Science Foundation) through the GREAT Research Network Programme. This research has made extensive use of NASA's Astrophysics Data System Bibliographic Services, and of the SIMBAD database and VizieR catalogue access tool, CDS, Strasbourg, France.

References

Anderson, J. & King, I. R. 2003, AJ, 126, 772
Armandroff, T. E. & Zinn, R. 1988, AJ, 96, 92
Baumgardt, H., Makino, J., & Hut, P. 2005, ApJ, 620, 238
Bekki, K. 2010, ApJ, 724, L99
Bellazzini, M., Bragaglia, A., Carretta, E., et al. 2012, A&A, 538, A18
Bellazzini, M., Ibata, R. A., Chapman, S. C., et al. 2008, AJ, 136, 1147
Bianchini, P., Varri, A. L., Bertin, G., & Zocchi, A. 2013, ApJ, 772, 67
Bradford, J. D., Geha, M., Muñoz, R. R., et al. 2011, ApJ, 743, 167
Carretta, E., Bragaglia, A., Gratton, R., D'Orazi, V., & Lucatello, S. 2009a, A&A, 508, 695
Carretta, E., Bragaglia, A., Gratton, R., & Lucatello, S. 2009b, A&A, 505, 139
Carretta, E., Bragaglia, A., Gratton, R. G., et al. 2014, A&A, 564, A60
Carretta, E., Bragaglia, A., Gratton, R. G., et al. 2006, A&A, 450, 523
Carretta, E., Bragaglia, A., Gratton, R. G., et al. 2009c, A&A, 505, 117
Carretta, E., Gratton, R. G., Lucatello, S., et al. 2010, ApJ, 722, L1
Carretta, E., Lucatello, S., Gratton, R. G., Bragaglia, A., & D'Orazi, V. 2011, A&A, 533, A69
Chen, C. W. & Chen, W. P. 2010, ApJ, 721, 1790
Cote, P., Welch, D. L., Fischer, P., & Gebhardt, K. 1995, ApJ, 454, 788
Da Costa, G. S. 1982, AJ, 87, 990
Djorgovski, S. & King, I. R. 1984, ApJ, 277, L49
Donati, P., Cantat Gaudin, T., Bragaglia, A., et al. 2014, A&A, 561, A94
Drukier, G. A., Bailyn, C. D., Van Altena, W. F., & Girard, T. M. 2003, AJ, 125, 2559
Dubath, P., Meylan, G., & Mayor, M. 1997, A&A, 324, 505

Ernst, A., Glaschke, P., Fiestas, J., Just, A., & Spurzem, R. 2007, MNRAS, 377, 465
Francois, P. 1991, A&A, 247, 56
Frinchaboy, P. M., Allende Prieto, C., Beers, T. C., et al. 2012, in American Astronomical Society Meeting Abstracts, Vol. 219, American Astronomical Society Meeting Abstracts #219, 428.04
Frinchaboy, P. M., O'Connell, J., Meszaros, S., et al. 2013a, in American Astronomical Society Meeting Abstracts, Vol. 221, American Astronomical Society Meeting Abstracts #221, 250.34
Frinchaboy, P. M., Thompson, B., Jackson, K. M., et al. 2013b, ApJ, 777, L1
Gilmore, G., Randich, S., Asplund, M., et al. 2012, The Messenger, 147, 25
Gnedin, O. Y., Lee, H. M., & Ostriker, J. P. 1999, ApJ, 522, 935
Goldsbury, R., Richer, H. B., Anderson, J., et al. 2010, AJ, 140, 1830
Goodwin, S. P. 1997, MNRAS, 286, L39
Gratton, R. G., Carretta, E., & Bragaglia, A. 2012, A&A Rev., 20, 50
Harris, W. E. 1996, AJ, 112, 1487
Ibata, R., Nipoti, C., Sollima, A., et al. 2013, MNRAS, 428, 3648
Jeffries, R. D., Jackson, R. J., Cottaar, M., et al. 2014, A&A, 563, A94
Kacharov, N., Bianchini, P., Koch, A., et al. 2014, ArXiv e-prints
King, I. 1961, AJ, 66, 68
King, I. R. 1966, AJ, 71, 64
Koposov, S. E., Gilmore, G., Walker, M. G., et al. 2011, ApJ, 736, 146
Kouwenhoven, M. B. N. & de Grijs, R. 2008, A&A, 480, 103
Lane, R. R., Kiss, L. L., Lewis, G. F., et al. 2009, MNRAS, 400, 917
Lane, R. R., Kiss, L. L., Lewis, G. F., et al. 2010a, MNRAS, 401, 2521
Lane, R. R., Kiss, L. L., Lewis, G. F., et al. 2010b, MNRAS, 406, 2732
Lane, R. R., Kiss, L. L., Lewis, G. F., et al. 2011, A&A, 530, A31
Lanzoni, B., Mucciarelli, A., Origlia, L., et al. 2013, ApJ, 769, 107
Lee, Y.-W. 1990, ApJ, 363, 159
Longaretti, P.-Y. & Lagoute, C. 1997, A&A, 319, 839
Lupton, R. 1993, Statistics in theory and practice
Lützgendorf, N., Kissler-Patig, M., Gebhardt, K., et al. 2012, A&A, 542, A129
Lützgendorf, N., Kissler-Patig, M., Noyola, E., et al. 2011, A&A, 533, A36
Mackey, A. D. & van den Bergh, S. 2005, MNRAS, 360, 631
Mastrobuono-Battisti, A. & Perets, H. B. 2013, ApJ, 779, 85
McLaughlin, D. E., Anderson, J., Meylan, G., et al. 2006, ApJS, 166, 249
McNamara, B. J., Harrison, T. E., & Anderson, J. 2003, ApJ, 595, 187
Mészáros, S., Holtzman, J., García Pérez, A. E., et al. 2013, AJ, 146, 133
Meylan, G. & Heggie, D. C. 1997, A&A Rev., 8, 1
Milone, A. P., Piotto, G., Bedin, L. R., & Sarajedini, A. 2008, Mem. Soc. Astron. Italiana, 79, 623
Munari, U., Sordo, R., Castelli, F., & Zwitter, T. 2005, A&A, 442, 1127
Nelder, J. A. & Mead, R. 1965, Computer Journal, 7, 308
Noyola, E. & Gebhardt, K. 2006, AJ, 132, 447
Pancino, E., Bellazzini, M., & Marinoni, S. 2013, Mem. Soc. Astron. Italiana, 84, 83
Pancino, E., Galfo, A., Ferraro, F. R., & Bellazzini, M. 2007, ApJ, 661, L155
Perryman, M. A. C., de Boer, K. S., Gilmore, G., et al. 2001, A&A, 369, 339
Plummer, H. C. 1911, MNRAS, 71, 460
Pryor, C. & Meylan, G. 1993, in Astronomical Society of the Pacific Conference Series, Vol. 50, Structure and Dynamics of Globular Clusters, ed. S. G. Djorgovski & G. Meylan, 357
Randich, S., Gilmore, G., & Gaia-ESO Consortium. 2013, The Messenger, 154, 47
Robin, A. C., Reylé, C., Derrière, S., & Picaud, S. 2003, A&A, 409, 523
Scarpa, R., Marconi, G., Carraro, G., Falomo, R., & Villanova, S. 2011, A&A, 525, A148
Shawl, S. J. & White, R. E. 1986, AJ, 91, 312
Siebert, A., Williams, M. E. K., Siviero, A., et al. 2011, AJ, 141, 187
Simmerer, J., Feltzing, S., & Primas, F. 2013, A&A, 556, A58
Sollima, A., Beccari, G., Ferraro, F. R., Fusi Pecci, F., & Sarajedini, A. 2007, MNRAS, 380, 781
Sollima, A., Bellazzini, M., Smart, R. L., et al. 2009, MNRAS, 396, 2183
Spurzem, R. & Einsel, C. 1999, in Astronomical Society of the Pacific Conference Series, Vol. 182, Galaxy Dynamics - A Rutgers Symposium, ed. D. R. Merritt, M. Valluri, & J. A. Sellwood, 105
Steinmetz, M., Zwitter, T., Siebert, A., et al. 2006, AJ, 132, 1645
Stetson, P. B. 1987, PASP, 99, 191
Stetson, P. B. 1992, in Astronomical Society of the Pacific Conference Series, Vol. 25, Astronomical Data Analysis Software and Systems I, ed. D. M. Worrall, C. Biemesderfer, & J. Barnes, 297
Trager, S. C., Djorgovski, S., & King, I. R. 1993, in Astronomical Society of the Pacific Conference Series, Vol. 50, Structure and Dynamics of Globular Clusters, ed. S. G. Djorgovski & G. Meylan, 347
Valdes, F. G. 1998, in Astronomical Society of the Pacific Conference Series, Vol. 145, Astronomical Data Analysis Software and Systems VII, ed. R. Albrecht, R. N. Hook, & H. A. Bushouse, 53
van de Ven, G., van den Bosch, R. C. E., Verolme, E. K., & de Zeeuw, P. T. 2006, A&A, 445, 513
van den Bergh, S. 2008, AJ, 135, 1731
van den Bosch, R., de Zeeuw, T., Gebhardt, K., Noyola, E., & van de Ven, G. 2006, ApJ, 641, 852
van der Marel, R. P. & Anderson, J. 2010, ApJ, 710, 1063
van Leeuwen, F., Le Poole, R. S., Reijns, R. A., Freeman, K. C., & de Zeeuw, P. T. 2000, A&A, 360, 472
Varri, A. L. & Bertin, G. 2012, A&A, 540, A94
Watkins, L. L., van de Ven, G., den Brok, M., & van den Bosch, R. C. E. 2013, MNRAS, 436, 2598
White, R. E. & Shawl, S. J. 1987, ApJ, 317, 246
Zocchi, A., Bertin, G., & Varri, A. L. 2012, A&A, 539, A65
Zucker, D. B., De Silva, G., Freeman, K. C., Bland-Hawthorn, J., & HERMES Team. 2013, in American Astronomical Society Meeting Abstracts, Vol. 221, American Astronomical Society Meeting Abstracts #221, 234.06
Zwitter, T., Siebert, A., Munari, U., et al. 2008, AJ, 136, 421